

UCRL-JC-114072
PREPRINT

Spectral Characterization of Lithographic Sources

C. Cerjan

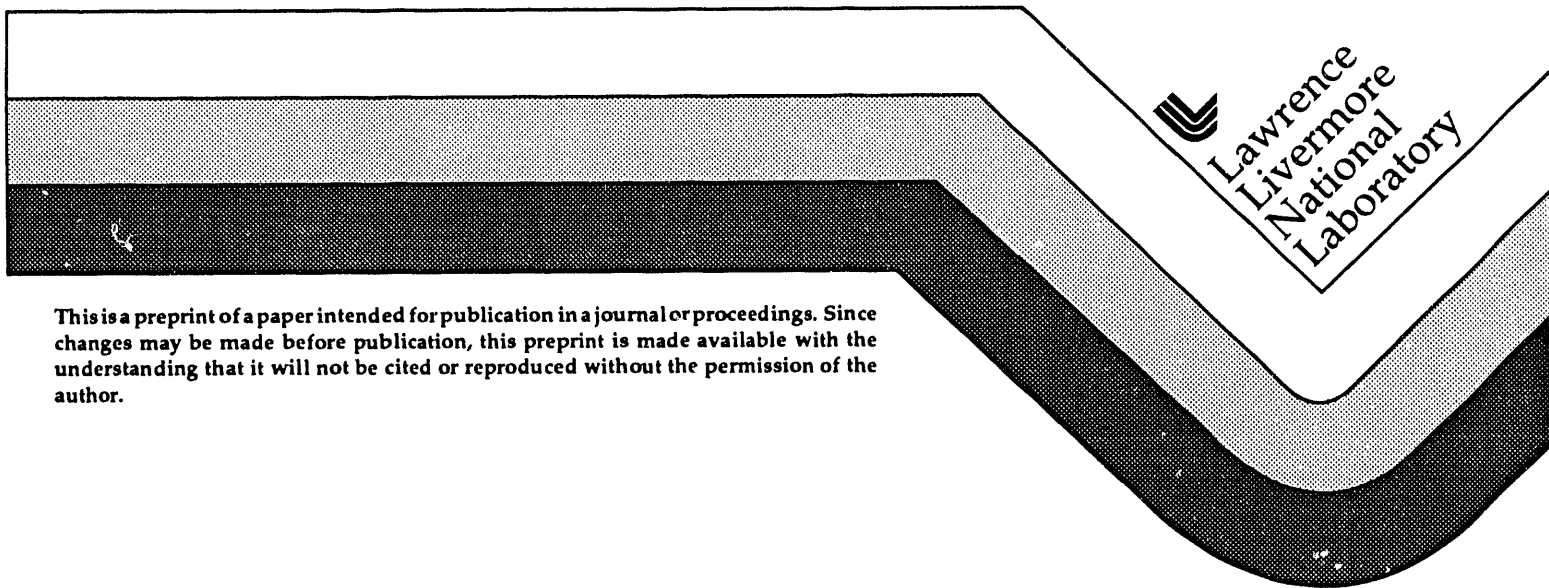
This paper was prepared for submittal to the
OSA Topical Meeting on Soft X-Ray
Projection Lithography ('93)
Monterey, California
May 10-12, 1993

June 1993

SEP 03 1993

OSTI

 Lawrence
Livermore
National
Laboratory



This is a preprint of a paper intended for publication in a journal or proceedings. Since changes may be made before publication, this preprint is made available with the understanding that it will not be cited or reproduced without the permission of the author.

MASTER

DISTRIBUTION OF THIS DOCUMENT IS UNLIMITED

Handwritten initials

DISCLAIMER

This document was prepared as an account of work sponsored by an agency of the United States Government. Neither the United States Government nor the University of California nor any of their employees, makes any warranty, express or implied, or assumes any legal liability or responsibility for the accuracy, completeness, or usefulness of any information, apparatus, product, or process disclosed, or represents that its use would not infringe privately owned rights. Reference herein to any specific commercial products, process, or service by trade name, trademark, manufacturer, or otherwise, does not necessarily constitute or imply its endorsement, recommendation, or favoring by the United States Government or the University of California. The views and opinions of authors expressed herein do not necessarily state or reflect those of the United States Government or the University of California, and shall not be used for advertising or product endorsement purposes.

Spectral Characterization of Lithographic Sources

C. Cerjan

POB 808, L-296

Lawrence Livermore National Laboratory

Livermore, CA 94550

Abstract

Spectral data collected in recent laser-plasma experiments at LLNL for Sn are compared to simulation results in order to more fully characterize the plasma properties, especially electron temperature and density. These plasma conditions determine the ionization states achieved by the material and the consequent radiative emission. Synthetic spectra are produced using very detailed radiating line positions and oscillator strengths calculated from extensive multi-configuration Dirac-Fock computations. Better quantitative agreement with experimental conversion efficiencies in the laser intensity regime of interest to projection soft x-ray lithography is obtained using this atomic database. The spectral characterization thus validates the general reliability of the simulations.

1. Introduction

A primary consideration in the design of an economically viable soft x-ray projection lithography scheme is the attainment of relatively high conversion efficiencies, ≈ 0.01 , within a relatively narrow spectral bandwidth, ≈ 0.022 centered at 134\AA^1 . These design constraints are dictated by the photon flux (conversion efficiency) required for the desired wafer throughput and by the choice of the Mo/Si multilayer optical components for the spectral output range. Although several x-ray sources show promise in meeting these requirements,

the investigation described below is directed toward the development of a laser-produced plasma source for the x-rays. Specifically, the research hopes to provide a more complete understanding of the plasma properties which produce high conversion efficiency within the narrow spectral band.

Conversion of the incident laser light into higher energy photon emission in a laser-produced plasma relies on the attainment of the appropriate ionization stages of the ionized species at a suitable electron density. The target material acts a nonlinear optical material which shifts the frequency of the incident light. As in other nonlinear optical materials, a relatively severe energy budget constraint is imposed by the relative inefficiency of the conversion. Laser energy is absorbed by the material which heats, expands, and ablates. The expansion and the ablation represent loss mechanisms in the energy balance since this energy does not reappear as re-radiated light. Thermal conduction which heats the material is also generally inefficient since this process fundamentally involves electron collisions which ionize the expanding material over a broad range of ionization states. Relatively few of these states contribute to the desired spectral output band; furthermore, the appropriate states are only produced for the approximate duration of the laser pulse.

An essential component of the underlying re-radiation mechanism is the assignment of the spectral lines within the desired bandwidth and an estimate of their oscillator strengths. These quantities are the fundamental quantum mechanical observables relevant to the emission of radiation. Consequently, these quantities must be accurately known before a reliable estimate of the spectral output can be made. Since the radiative output is very sensitive to both the plasma characteristics and to the atomic data, the comparison of synthetic spectra to the experimentally observed spectra provides a stringent test of a simulation's reliability.

The investigations described below attempt such a spectral characterization in the case of Sn solid targets irradiated by a Nd-YAG laser system at intensities relevant to a proposed point-projection lithography scheme¹. The following section presents a brief overview of the photon conversion mechanism in laser-produced plasmas. The third section contains a description of the simulations performed for the conditions mentioned above, including

the overall conversion efficiencies expected and a comparison of the synthetic spectra to the experimental spectra. The final section describes the limitations of the present study and offers some general conclusions.

2. Review of Radiating Plasmas

In this brief discussion, attention will be focussed on the generation of those plasma conditions initiated by laser deposition which produce radiation useful for projection lithographic applications. The general outline of the effort is clear: establish the appropriate emitting stages of the target material for the longest duration in an optically thin portion of the plasma. The two controlling plasma parameters are the electron temperature and density. These quantities are directly related to the choice of target material, for the allowed emitting states, and the laser parameters - especially energy deposited, pulse length and focal spot size. The laser parameters determine the rate of ablation and amount of collisional heating which in turn control the conversion efficiency into a selected output band. The optimization of this conversion efficiency is, of course, a major objective of the source design.

The laser intensity regime of interest in the current application is moderate: ranging from approximately 10^{10} to $10^{13} \text{Watts/cm}^2$. This regime is intermediate between laser welding applications, 10^8 to 10^9Watts/cm^2 , and inertial confinement fusion requirements, 10^{14} to $10^{16} \text{Watts/cm}^2$. The lower intensity regime is not appropriate because of the low temperatures achieved and large opacity effects. The corresponding difficulties with the higher intensity conditions is the possible onset of plasma instabilities which seriously compromise the energy deposition. In the intermediate regime, then, there are essentially two contributions to the energy balance: the hydrodynamic expansion, which represents an energy loss mechanism by cooling, and the radiative emission.

The goal in source optimization is to restrict the hydrodynamic losses by producing a collimated plasma with relatively little lateral expansion during the rapid ablation phase. This energy is then available to promote collisional ionization of the target material leading

to enhanced photon production. Minimizing the expansion energy loss of course does not automatically provide an optimal source since the ionized material must possess strong radiative transitions in the spectral range of interest. This latter consideration underscores the importance of the target material choice.

A summary of the experimental parameters and their relative effect on the plasma conditions created is presented in Table 1. The critical electron density at which maximal laser absorption occurs is controlled by the laser light frequency which is inversely proportional to the second power of the wavelength². The physical scale-length of the plasma is set by this density; a lower critical density implies a larger plasma region. Furthermore, a higher density at absorption implies shorter photon mean free paths and radiation trapping becomes important. The time-scale for electron thermal conduction is determined by the laser temporal pulse duration. Since the deposition mechanism is absorption of laser light, the electrons will be heated during the pulse and thereafter will only cool by expansion in the optically thin region. The plasma will remain approximately collimated during the laser pulse if the ablated material moving at the local sound speed does not exceed the laser focal diameter². Thus the plasma conditions should scale with the ratio of laser energy per area provided this dimensionality constraint is satisfied³. As the focal spot becomes smaller at fixed energy and pulse length, a transition between cylindrical and spherical expansion will occur. At this point, hydrodynamic losses will degrade the conversion efficiency. Within the cylindrical expansion regime, a change in the laser intensity most directly affects the electron temperature which in turn will change the ionization states accessed during plasma production. Finally, as mentioned above, the atomic number of the target material influences the charge states possible by collisional ionization and the line positions and strengths during emission. Low atomic number materials produce sharp, line spectra; high atomic number materials produce broad, diffuse spectra since there are relatively more ionization states with possibly closely spaced, high multiplicity configurations.

Some simple scaling relationships can quantify these comments further. In the low-intensity regime, assuming collimated expansion of the plasma, one such self-similar relation

has been derived by Mora³

$$T_e \cong 60.5 \left(\frac{I}{4.8 \times 10^{11}} \right)^{1/2} \left(\frac{\lambda}{1.064} \right)^{1/2} \left(\frac{2Z}{A} \right)^{-1/8} \left(\frac{\bar{Z}\Lambda\tau}{0.1} \right)^{1/4}, \quad (1)$$

where the electron temperature, T_e , is expressed in *eV*; the intensity, I , is in *Watts/cm²*; the laser wavelength, λ , is in μm ; Z is the dominant charge state; A is the atomic number of the material; \bar{Z} is the average charge of the plasma; Λ is the scaled Coulomb logarithm; and τ is the laser pulse duration in *ns*. This equation summarizes the interplay among the various experimental parameters. For example, for fixed pulse-length, laser energy and material, the electron temperature is expected to scale inversely as the focal radius. This scaling can be expected to fail when the collimation of the ablating plasma degrades. Thus a series of experiments with changing focal spot size will locate the transition between cylindrical and spherical expansion.

As an illustration of this transition, the electron temperatures as a function of laser intensity for the particular case of Sn at 1064 nm can be predicted and compared to two-dimensional LASNEX simulations⁴. Using the specific values of $Z = \bar{Z} = 15$, $\lambda = 1064nm$, $\Lambda = 1.0$, and $\tau = 7.5ns$, the dependence of the electron temperature on intensity is

$$T_e \cong 2.63 \times 10^{-4} I^{1/2}. \quad (2)$$

The comparison to the simulated peak electron temperatures is displayed in Table 2. These results demonstrate that the simple scaling relation begins to fail between 1×10^{11} and $5 \times 10^{11} Watts/cm^2$, signalling the transition to spherical expansion. The simulation temperatures are of course lower since more energy is expended in material expansion than is anticipated by the scaling relation. For the stated conditions, the focal radius at which this transition occurs is $125 \mu m$ at $2 \times 10^{11} Watts/cm^2$ for a laser energy of $0.3 J$. This value is in reasonable agreement with observations⁵.

The optimization of photon production into the narrow band also relies critically on the atomic number of the target material. If the electron density is sufficiently low, the balance between electron collisional effects and photon emission and absorption will be shifted toward

the escape of photons from the plasma. This shift indicates that the plasma is no longer in local thermodynamic equilibrium, hence the plasma becomes a useful source of light. Since free-free and free-bound electronic transitions are continuous in energy (translational motion is not quantized), the radiation expected from these transitions will be more diffuse and less important in producing narrow band output. On the other hand, bound-bound transitions will concentrate the emitted photons into output bands that are only slightly broadened by Doppler motion. Clearly these latter effects are most desirable for the intended source.

The power emitted into a line, P_{line} , from a cylindrical source can be expressed as⁶

$$P_{line} = 7 \times 10^{-25} \frac{n_e n_{ig}}{T_e^{1/2}} \sum_n f_{ni} \exp(-E_n/T_e). \quad (3)$$

The transition energy, E_n , and temperature are given in eV; the electron density and ion ground-state density, n_{ig} , are given in *particles/cm³*; f_{ni} is the emission oscillator strength for the transition $n \rightarrow i$; and the power is given in units of $\frac{J}{cm^3 sec}$. The summation includes all those transitions contributing to the specified photon energy. The qualitative features required for optimization of this power are clearly represented in this expression. The population of the relevant ionization states, $n_{ig} \exp(-E_n/T_e)$, should be high; the oscillator strengths should be large; and there should be many transitions contributing to the summation.

These general considerations delineate the expected features of an optimized laser-produced plasma source. Simple scaling relations of course do not suffice for a detailed comparison with experimental results; likewise the power emitted is a time-dependent quantity which varies in a complicated fashion with time and space. The role of more extensive computer simulations is to include these temporal and spatial variations in the plasma to obtain a more faithful representation of the underlying processes.

3. Simulation Results

A simulation of the evolving plasma is a demanding task, requiring realistic models for the cold material thermodynamic properties; the solution of the mass continuity, momentum

balance and energy conservation equations; a reasonable treatment of radiation transport; and accurate atomic rate data. To complicate matters further, these phenomena are intrinsically coupled. A computational tool has been developed for laser inertial confinement fusion, the LASNEX code⁷, which can be extended to the intensity regime required for projection lithographic plasma sources. A brief description of this tool has been provided earlier for similar, less extensive calculations⁴. For the present investigation, it should be mentioned that these simulations were performed in cylindrical geometry with a detailed atomic rate database.

The development of this database is the principal difference between those earlier simulations and the work reported here. Relatively accurate line positions and oscillator strengths are required so an *ab initio* approach was chosen. The multi-configuration Dirac-Fock code⁸ was applied to construct a highly detailed set of excitation energy levels and oscillator strengths for the ionization states Sn^{+4} to Sn^{+18} . Electron collisional rates were included by using various semi-empirical fits⁹. Substantial configuration mixing was observed which increased the complexity of the calculations especially for the $\Delta n = 0$ transitions. An additional difficulty arose from the size of the database which exceeded practical disk storage limits; this problem was overcome by configuration averaging which reduced the database with the loss of some fine detail in the spectroscopic characterization. Dielectronic recombination was included in an approximate manner by introducing averaged transition radiative decay rates to the neighboring ground ionization state.

Several prominent spectral features were identified. Low energy (140-147 Å) excitations were assigned to 4f-4d transitions in Sn^{+6} to Sn^{+10} . The Mo/Si multilayer range (127-134 Å) was assigned to 4d-4p transitions in Sn^{+10} to Sn^{+14} and 4f-4d transitions in Sn^{+11} to Sn^{+13} . Finally, a high energy feature (76-82 Å) was assigned to 5s-4p transitions in Sn^{+12} to Sn^{+14} . A great wealth of other spectral information could be derived from this database, but the current experimental resolution⁵ cannot distinguish finer spectral detail.

The conversion efficiency at 134 Å into a 0.022 bandwidth can be calculated using this amassed data. The simulations adopted the experimental parameters wherever possible⁵.

For the optimized conditions, the target material was Sn irradiated by 1064 *nm* light, energy 0.3 *J*, pulse full-width half-maximum of 7.5 *ns*, with a changing focal diameter. The comparison between the experimental and simulated conversion efficiencies are plotted as a function of laser intensity in Fig. 1. The experimental trend is clearly reproduced with the experimental values lying consistently higher than the simulations. The discrepancy is particularly pronounced at higher intensities where the simulations drop much more rapidly as a function of intensity.

Spectral characterization was also attempted by producing synthetic spectra. In Fig. 2 four different intensity experimental spectra are plotted as a function of photon energy for the above laser conditions. There are two largely unresolved features in these plots: a lower energy band between 80 and 90 eV and a high energy feature centered at 150 eV. The emergence of the high energy feature is a clear signature of the higher electron temperature achieved at higher intensity. A more subtle feature is the sharpening of the peak between 80 and 90 eV as the lower ionization state populations contribute less at the higher intensities so that they provide less radiative output. These features are reproduced by the simulations in Fig. 3 and Fig. 4.

As a final example of the spectral characterization, the simulation was repeated for Sn at 532 *nm* with a laser energy of 1.0 *J* and an intensity of $1.4 \times 10^{11} \text{Watts/cm}^2$. The synthetic spectrum is plotted in Fig. 5 which is more similar to the 1064 *nm* result at $5.7 \times 10^{10} \text{Watts/cm}^2$ than it is to the higher intensity result in Fig. 4. The feature at 150 eV is clearly suppressed at shorter wavelength and the low energy spectral output is higher than that in Fig. 4. This result corroborates the claim⁵ that the shorter wavelength laser light is somewhat less efficient than 1064 *nm* light. Furthermore, the scaling relation for the electron temperature above suggests that this temperature should be lower at the same intensity.

4. Discussion and Conclusions

The inclusion of an extensive atomic rate database significantly increases the accuracy of the radiative output predictions. Several discrepancies remain though. First, the accuracy of the line positions and the configuration averaging technique employed cannot be assured to more than $\pm 2 \text{ \AA}$. The line positions themselves are limited by this uncertainty and the averaging procedure, though reasonable, might be skewed toward a non-representative set of configurations. Second, although the model is very extensive, it is necessarily incomplete. The inclusion of more configurations is probably necessary but cannot be accomplished given the practical limitations of computer storage and running speeds. This deficiency is especially important for dielectric recombination processes which cannot be calculated given their extensive nature for the 4d and 4f configurations. Third, the simulations predict more low energy spectral emission than is observed. This might be caused by detector response limits in the experiment or radiative transport effects in the denser, cooler regions of the plasma. Fourth, intermediate spectral output is predicted between 110 and 125 eV which is not resolved in the experiments. This discrepancy might be a reflection of inaccuracies in the radiative line position calculations. Finally, the atomic database extends only to Sn^{+18} which certainly induces inaccuracies at the higher laser intensities where higher lying ionization states are accessed. This fact probably contributes to the discrepancy in the conversion efficiency noted in Fig. 1.

In conclusion, the chief results of this investigation are as follows. The experimental trends for the conversion efficiency as a function of laser intensity and wavelength are confirmed. The spectra are expected to differ significantly between 1064 *nm* and 532 *nm* light but the peak conversion efficiencies do not differ substantially. The synthetic spectra confirm the characterization of the plasma parameters since low and high energy features arise in a similar fashion to the experiment. The appropriate ionizing states for these features have been assigned. The predicted spectral output is very sensitive to the choice of atomic transitions included; the accuracy in line position and oscillator strength critically limit the

predictive nature of the calculations.

ACKNOWLEDGMENTS

The author is pleased to acknowledge useful scientific discussions with Drs. M. Chen, J. Nash, and A. Osterheld concerning the atomic rate database. Thanks are due to the LAS-NEX group members, especially Drs. J. Harte, S. Wilson, and G. Zimmerman. Work at the Lawrence Livermore National Laboratory is performed under the auspices of the U. S. Department of Energy, administered by the University of California under Contract No. W-7405-Eng-48.

REFERENCES

1. N. M. Ceglio and A. M. Hawryluk, "Soft X-ray Projection Lithography Design," OSA Proceedings on Soft-x-ray Projection Lithography, v. 12, J. Bokor, ed., pp. 5-9, (Optical Society of America, Washington D. C., 1991).
2. G. E. Max, "Physics of the Coronal Plasma," in Les Houches, session XXXIV, 1980 - Interaction Laser-Plasma/Laser-Plasma Interaction, R. Balian and J. C. Adam, eds., pp. 302-410, (North-Holland, Amsterdam, 1982).
3. P. Mora, "Theoretical model of absorption of laser light by a plasma," Phys. Fluids, **25**, pp. 1051-1056(1982).
4. C. Cerjan, "X-ray Plasma Source Design Simulations," Appl. Op., (to appear); R. E. Olson, W. C. Sweatt, and P. D. Rockett, "Computational simulations of an SXPL laser plasma source," in this Proceedings.
5. R. C. Spitzer, R. L. Kauffman, T. Orzechowski, D. W. Phillion, and C. Cerjan, "X-ray production from laser-produced plasmas for SXPL applications," in this Proceedings.
6. H. Griem, "Plasma Spectroscopy," Chp. 7 (McGraw-Hill, New York, 1964).
7. G. B. Zimmerman and W. L. Kruer, "Numerical Simulation of Laser Initiated Fusion," Comm. Plasma Phys. Cont. Thermonuclear Fusion, **2**, 85(1975).
8. I. P. Grant, B. J. McKenzie, P. H. Norrington, D. F. Mayers, and N. C. Pyper, "An Atomic Multiconfigurational Dirac-Fock Package," Comp. Phys. Comm., **21**, 207-231(1980).
9. L. B. Golden, R. E. H. Clark, S. J. Goett, and D. H. Sampson, Ap. J. Suppl., **45**, 603(1981).

TABLES

Table 1. Experimental parameters and their physical effects

Parameter	Effect	Range
Laser frequency, ω	Absorption density	248, 532, 1063 nm
Laser pulse, τ	Conduction/emission time-scale	2 - 35 nsec
Laser energy/area, E/r_{foc}^2	Dimensionality ratio	0.2 - 1.0 J, $r_{foc} > 10\mu m$.
Laser intensity, I	Electron temperature	10^{10} to 10^{13} Watts/cm ²
Atomic number, Z	Radiative transitions	20 - 80 -

Table 2. Comparison of the electron temperature scaling relation with peak simulation values

Intensity (Watts/cm ²)	Scaling result (eV)	Simulation (eV)
5×10^{10}	57	65
1×10^{11}	83	81
5×10^{11}	181	120
1×10^{12}	257	180

FIGURES

Fig. 1. Conversion efficiency per eV as a function of laser intensity for the conditions given in the text.

Fig. 2. Experimental spectra for the four indicated intensities for the laser conditions given in the text.

Fig. 3. Synthetic spectra for an intensity of 5.7×10^{10} *Watts/cm²* using the laser conditions given in the text.

Fig. 4. Synthetic spectra for an intensity of 2.5×10^{11} *Watts/cm²* using the laser conditions given in the text.

Fig. 5. Synthetic spectra for an intensity of 1.4×10^{11} *Watts/cm²* using the laser conditions given in the text for 532 *nm* laser light.

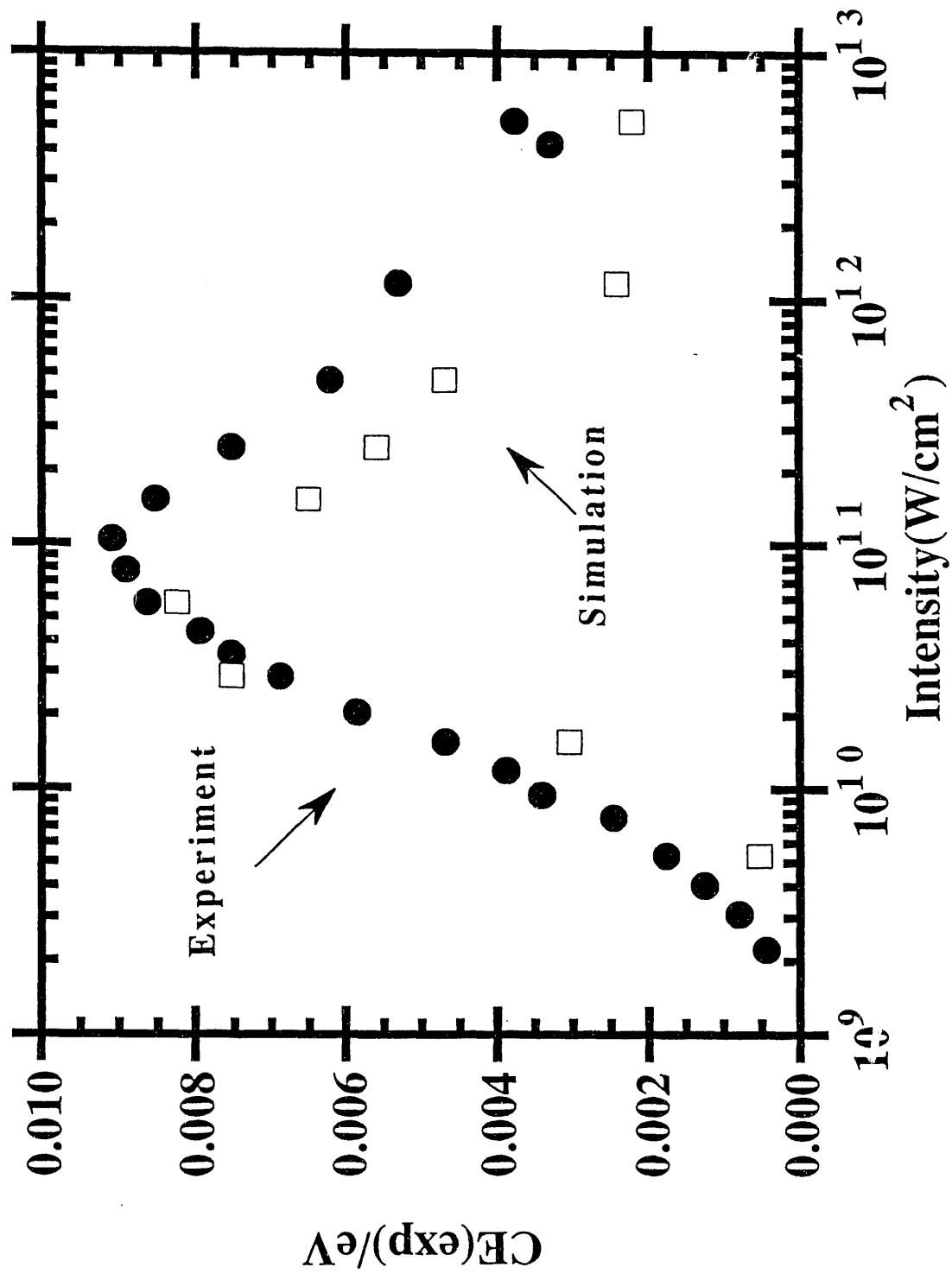


Figure 1

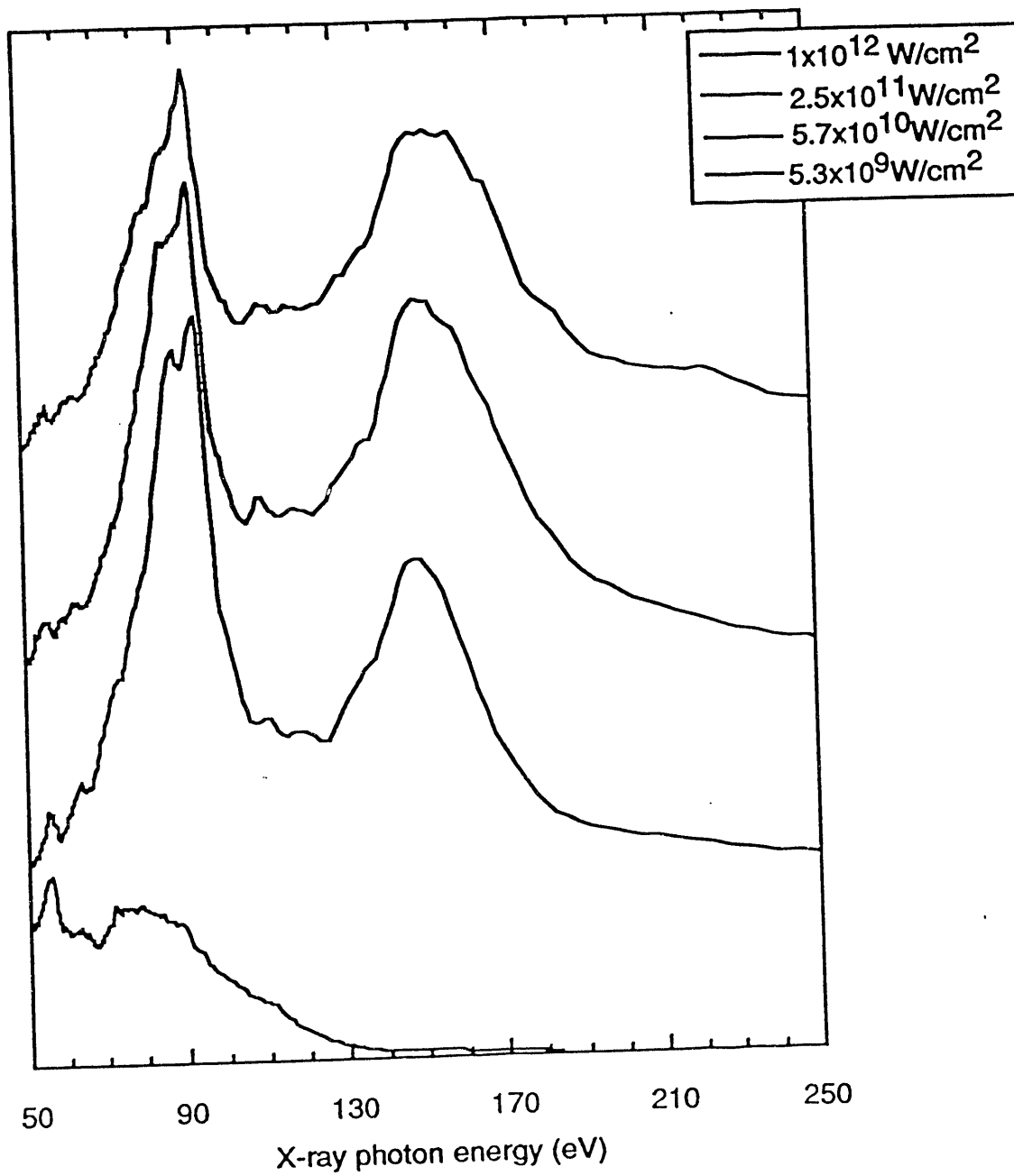
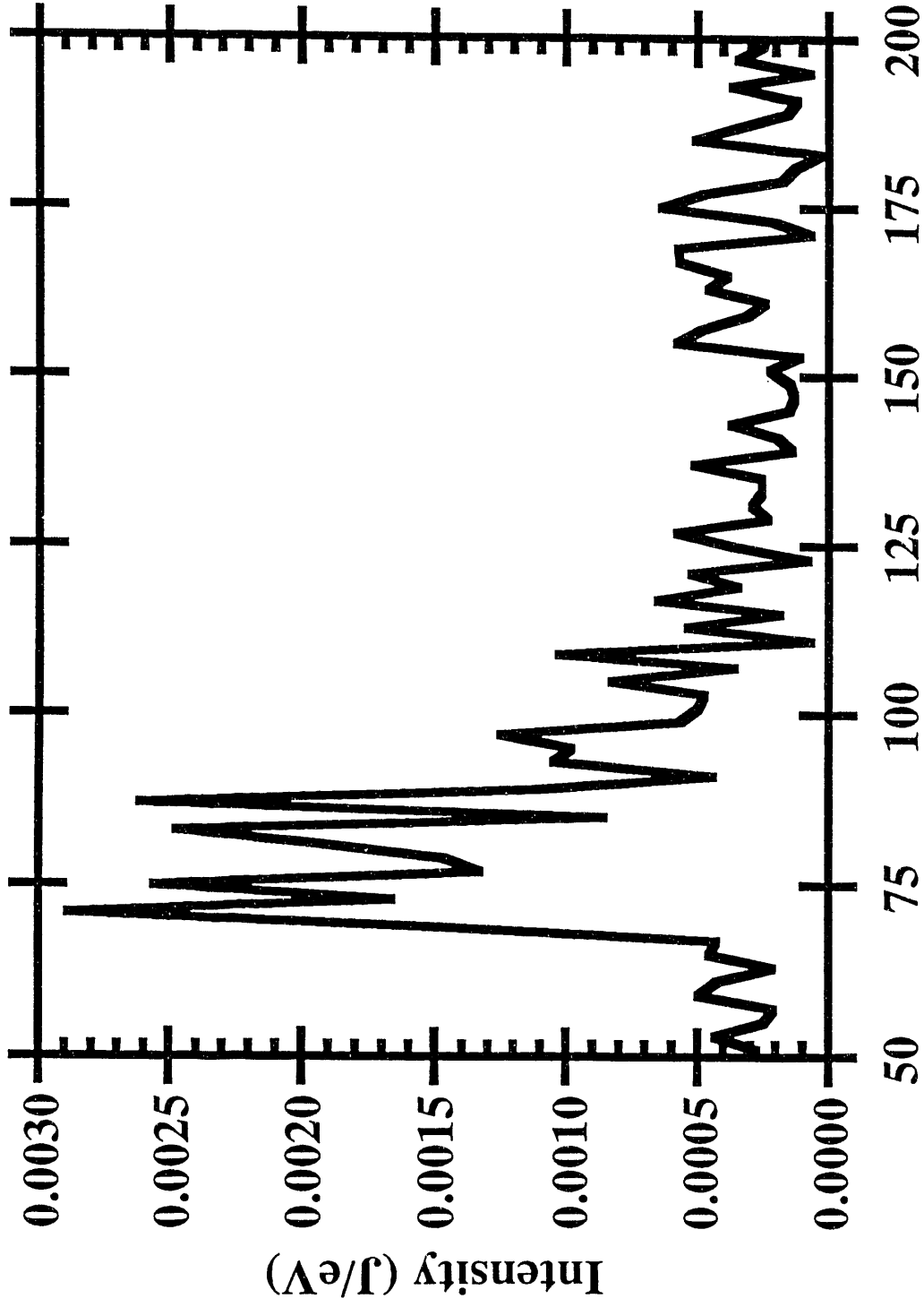
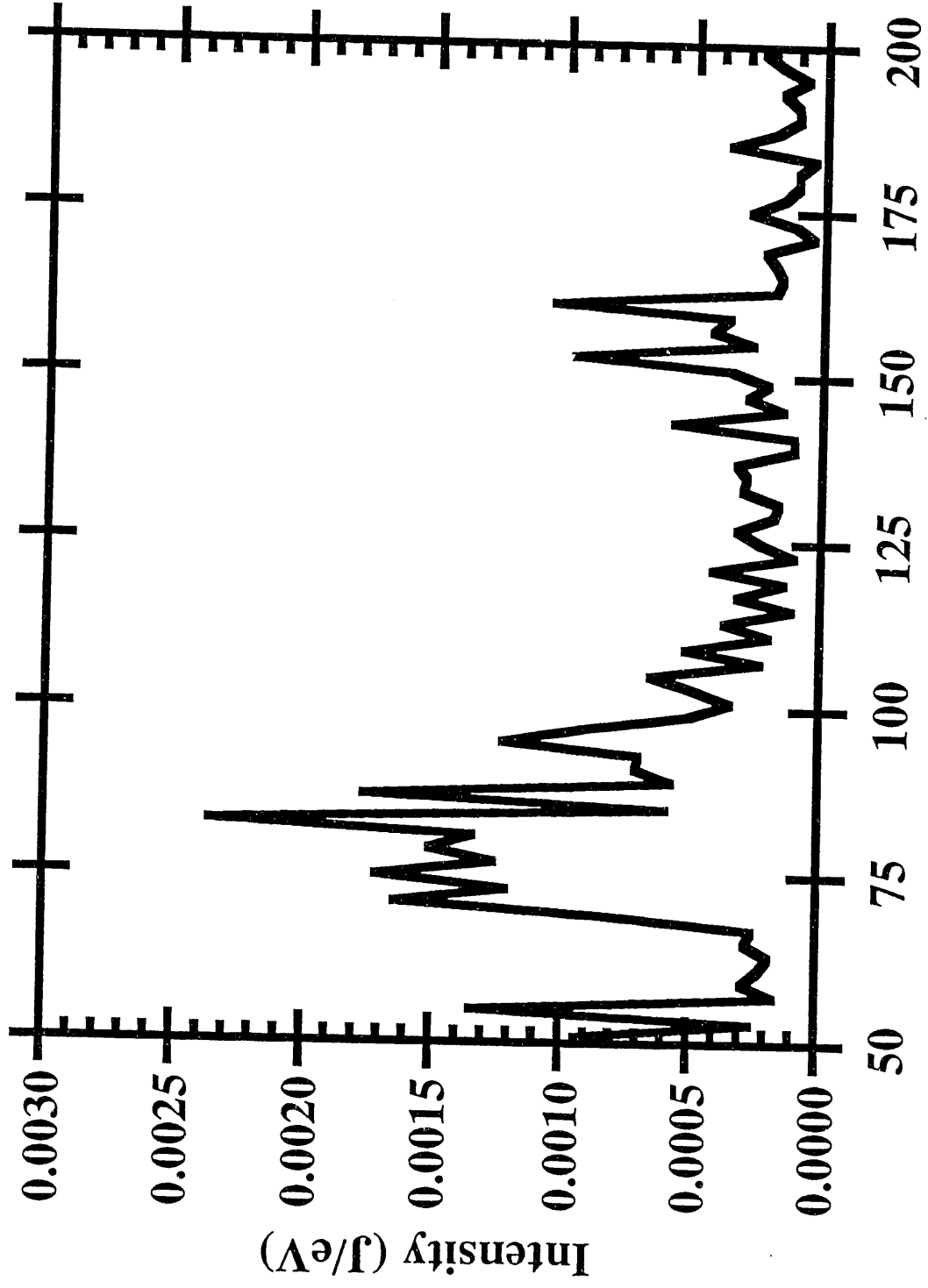


Figure 2

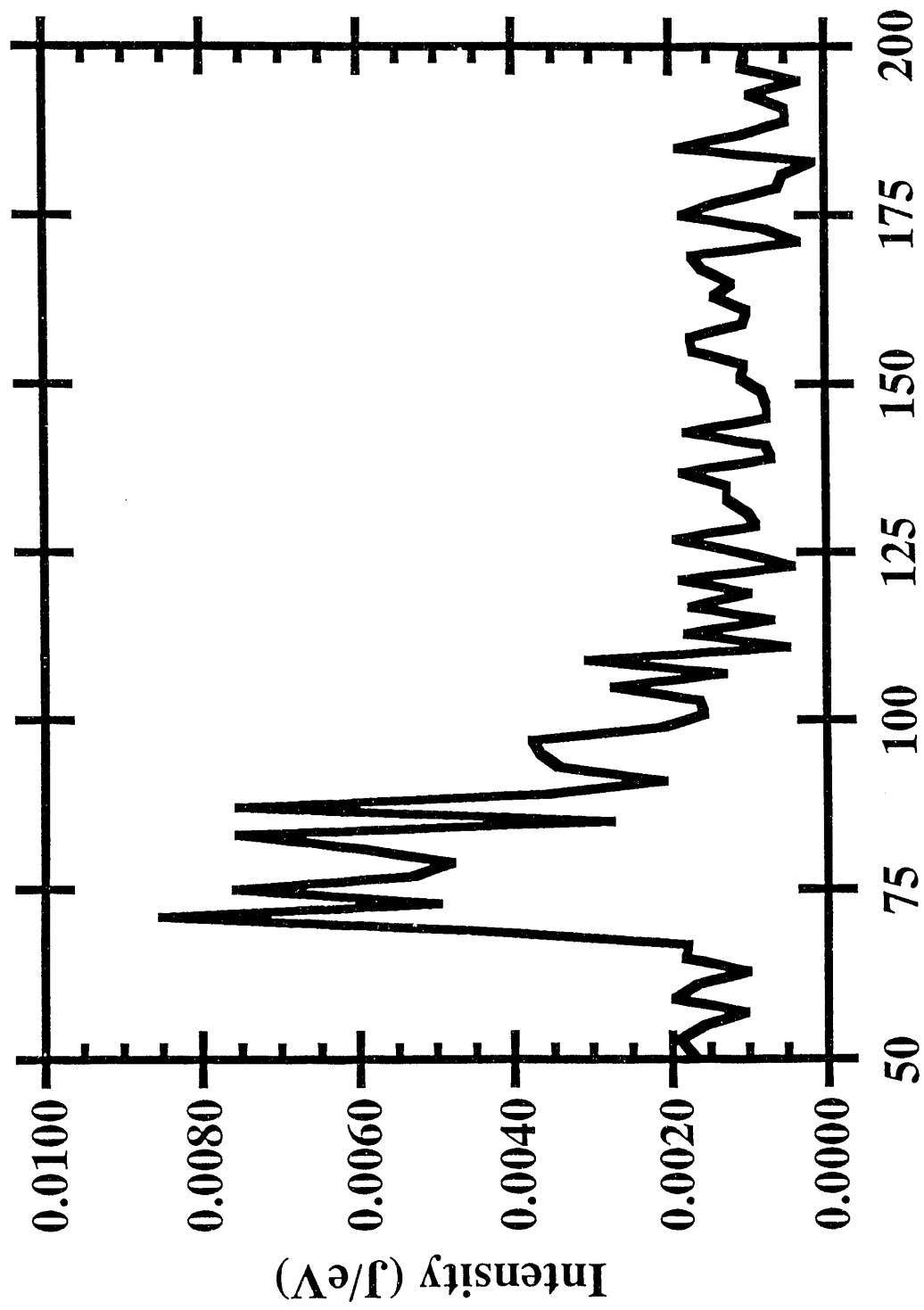


Energy (eV) Figure 3



Energy (eV)

Figure 4



Energy (eV) Figure 5

END

**DATE
FILMED**

11 / 16 / 193

